Journal of Imaging Informatics in Medicine
https://doi.org/10.1007/s10278-024-01076-z

DL-EDOF: Novel Multi-Focus Image Data Set and Deep Learning-Based Approach for More Accurate and Specimen-Free Extended Depth of Focus

Hulya Dogan[1,3] · Ramazan Ozgur Dogan[2] · Ilyas Ay[3] · Sena F. Sezen[3,4]

Received: 4 October 2023 / Revised: 9 November 2023 / Accepted: 13 November 2023

Abstract
Depth of focus (DOF) is defined as the axial range in which the specimen stage moves without losing focus while the imaging apparatus remains stable. It may not be possible to capture an image that includes the entire specimen in focus due to the narrow DOF in microscopic systems. Extended depth of focus (EDOF) is used to overcome this limitation in microscopic systems. Although the researchers have developed so many EDOF microscope approaches, this research field still has some crucial shortcomings such as high computational costs, complexity and execution time, requiring additional equipment, low precise characterization of curves, and edges in images, varying performance depending on the specimen and microscope, using only gray levels of input images to acquire the pixel's focus values. In order to minimize these shortcomings and comprehensively analyze the performance of EDOF approaches, a novel multi-focus image data set is generated, and a deep learning-based EDOF microscope approach is proposed in this study. When compared with the state-of-art EDOF approaches, our study provides various crucial contributions such as the first EDOF approach based on unsupervised deep learning, providing more accurate and specimen-free EDOF, generating a novel multi-focus image data, not requiring any pre- or post-processing technique and acquiring the pixel's focus degrees using deep features. In order to evaluate the effectiveness of the suggested approach, 20 different EDOF approaches are applied to a multi-focus image data set containing 9 image collections (4 synthetic and 5 microscope image collections) in total. Performance analysis metrics with and without requiring a reference image are preferred to identify which EDOF microscope approach can extract more essential details from the multi-focus images for the synthetic and microscope image collections, which are Root Mean Square Error (RMSE), Peak Signal Noise Ratio (PSNR), Universal Quality Index (UQI), Correlation Coefficient (CC), Perception-based Image Quality Evaluator (PIQE), Blind/Referenceless Image Spatial Quality Evaluator (BRISQUE), Extension of Universal Quality Index for N Images (UQIN), and Naturalness Image Quality Evaluator (NIQE). Objective and subjective analysis of this study demonstrates that unsupervised deep learning model is more efficient to transmit crucial details from multi-focus images. Moreover, the suggested EDOF microscope approach with highest PSNR, UQI, CC, UQIN and lowest RMSE, PIQE, BRISQUE, NIQE produces higher performance than the state-of-art approaches.

Keywords Extended depth of focus · Unsupervised deep learning · Focus measurement operator · Auto-encoder · Depth of focus · Microscopic system

Introduction

In microscopic systems, depth of focus (DOF) is described as the axial range in which the specimen stage moves without loss of focus while the imaging equipment remains stable. It is impossible to capture an image in which the full area of the specimen is focused when its size is wider than the microscope DOF. When scanning the specimen in the *Z*-axis, only the areas inside the DOF are clearly visible. Figure 1 shows multi-focus images with the same field of perspective and different areas in focus. As shown in Fig. 1, specimen areas that are not inside the DOF seem blurry. While developing applications such as classification, segmentation, registration, and stitching, which are performed using image processing and artificial intelligence algorithms in microscopic systems, researchers do not prefer the image (shown in Fig. 1), which is captured when the specimen size is wider than the DOF. In order to increase the effectiveness of image processing and artificial intelligence algorithms in microscopic systems, the image in which the full area of

Extended author information available on the last page of the article

Published online: 25 March 2024

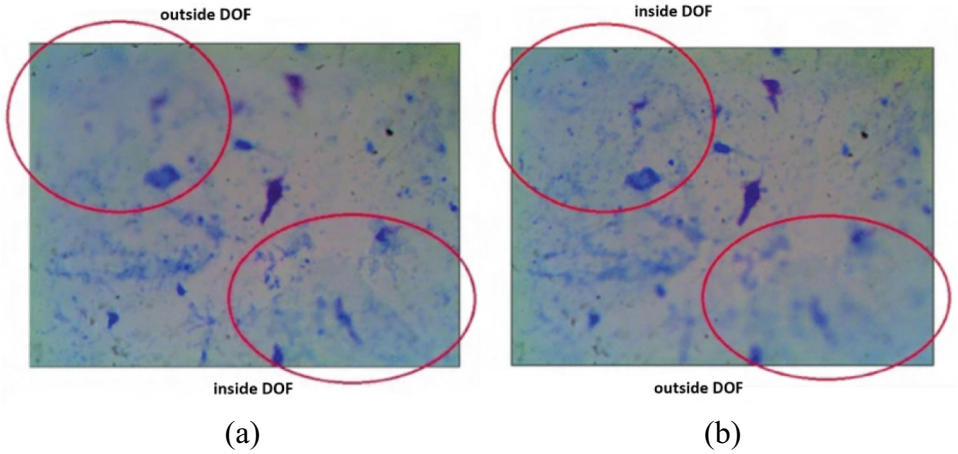

Fig. 1 Multi-focus images with the same field of perspective and different areas in focus

the specimen is focused is created with an extended depth of focus (EDOF) microscope.

In the literature, the approaches developed for EDOF microscope are divided into two categories: wavefront coding and image fusion based [1]. DOF is extended by placing elements on the back focusing plane of the microscope objective in the wavefront coding-based approaches, firstly generated by Dowski and Cathey [2]. Advantages: great precision and real-time performance. Disadvantages: high cost and requiring additional hardware [3–5]. On the other hand, image fusion-based approaches create an image in which the full area of the specimen is focused by using a collection of multi-focus images. According to literature researches, these approaches are the most frequently preferred to produce the image in which the full area of the specimen is focused in the microscope systems [6, 7]. Advantages: low cost and not requiring additional hardware. Disadvantages: performance variation according to the specimen and microscope. These approaches consist of three main phases:

1. Producing a collection of multi-focus images: By adjusting the specimen stage in the *Z*-axis during this phase, images with the same field of perspective and different areas in focus are captured.
2. Calculating pixel's focus values in the collection of multi-focus images: In this phase, the values giving information about the focusing of every pixel are calculated by focus measurement operators. The researchers categorize focus measurement operators into six classes [8]:
    - Based on Gradient: These operators use the pixel's first derivative to determine the focus value. Gaussian Derivative, Tenengrad, and Gradient Energy are some examples of these measurement operators that are frequently used in the literature.
    - Based on Laplacian: These operators use the pixel's second derivative to extract the focus value. Variance of Laplacian, Energy of Laplacian, Multi-Directional Modified Laplacian, and Laplacian in 3D can be given as examples of these measurement operators.
    - Based on Wavelet Transform: These operators utilize discrete wavelet transform coefficients to calculate the pixel's focus value. Sum of Wavelet Coefficient, 3D Wavelet Transform, and Variance of Wavelet Coefficient are some examples of these measurement operators generally used in the literature.
    - Based on Statistics: These operators use the image's quality data such as density and histogram to produce the pixel's focus value. Chebyshev Moments, Eigen Values, Variance, and Histogram Entropy are the popular statistics-based measurement operators.
    - Based on Cosine Transform: These operators utilize discrete cosine transform to compute the pixel's focus level. The common measurement operators are Discrete Cosine Transform (DCT) Reduced Energy Ratio and DCT Energy Ratio.
    - Others: These operators use the pixel's specific features to compute the focus degree. Local Binary Pattern, Spatial Frequency, Discrete Curvelet Transform, Brenner's Focus Measure, 2D and 3D Steerable Filters, Non-Subsampled Shearlet Transform, Gabor Features, Auto-correlation, and Image Curvature can be given as some examples of these measurement operators.
3. Selecting pixels with maximum focus value: In this phase, a single image is combined by selecting the pixels with maximum focus value in the collection of multi-focus images. In order to determine the pixels with maximum focus value, the researchers utilize fusion selection rules. Average and Maximum Selection can be given as examples for classical fusion selection rules.

Related Works

As stated previously, there are two categories of approaches proposed for EDOF microscope: wavefront coding and image fusion based. The examples of the studies proposing a wavefront coding-based approach can be given as follows: Dowski and Cathey created an optical-digital system offering image performance with a broad DOF that is nearly diffraction-limited [2]. Wavefront coding imaging technology with a cubic phase mask was introduced for EDOF microscope system [9]. In this system, the standard incoherent optical system was changed by a phase mask, and the resulting intermediate image was undergone digital processing. In order to create a wavefront-coding EDOF microscope system, Zhao et al. developed two major optimization techniques based on the commercial optical design software [10]. Gierlak et al. utilized a spatial light modulator to design a wavefront coding-based EDOF microscope [11]. In order to accomplish deblurring, a computerized imaging strategy was proposed for EDOF microscope [3]. This study implemented wavefront coding using diffractive optical element and convolutional neural network. Cao et al. suggested adding wavefront coding to the microscope system in order to enhance the system's performance while exposed to nonuniform spectrum [12]. In order to minimize the restrictions of EDOF microscope, a computational imaging-based technique was suggested by Elmalem et al. [13]. Du et al. suggested a technique named lens-combined wavefront coding to simultaneously increase the aperture and DOF [14]. Wei et al. constructed two alternative wavefront coding systems with the phase plate integrated in various optical system surfaces in order to observe the imaging properties of the integrated wavefront coding system [15]. By using a genetic algorithm, Li et al. proposed a high-order polynomial phase mask increasing success modulated transfer function defocus consistency [16].

Literature studies for image fusion-based approach can be exemplified as follows: Valdecasas et al. built a new method for computing the EDOF, where three different tests and ten alternative methods were utilized for the proposed method evaluation and test [17]. An approach based on image formation model assessing jointly a specimen's texture and topography from a collection of bright-field optical sections was proposed by Aguet et al [18]. In order to extract the focusing characteristics from the image collection produced by the microscopic system, Forster et al. devised an approach based on the complex value discrete wavelet transform (CDWT) [19]. It has been noted in the literature studies, nonetheless, that CDWT has some restrictions when it comes to retrieving curve and edge information from images. Tessens et al. developed an EDOF technique using discrete curvelet transform (DCT) to minimize these restrictions [20]. According to Forster and Tessen's findings, the dimensions of the frequency coefficients derived by CDWT and DCT differ from the dimensions of the multi-focus images. This causes the focusing information to not be adequately extracted from multi-focus images. Dogan et al. proposed a new approach based on non-subsampled shearlet transform (NSST) for EDOF in microscopic systems, which has faster and better sparse representation than existing multiscale transforms (CDWT, DCT) [21]. To generate an EDOF microscope image with every bacillus visible in microscope, a multi-focus image fusion method was proposed in [22]. Using synthetic sets of images with ground truth, Piccinini et al. devised a novel technique for EDOF microscope [23]. The researchers utilize fusion selection rules, as discussed earlier, to identify the pixels with the highest focus value. In addition to classical fusion selection rules (Average and Maximum Selection), since the focusing characteristics are calculated using low and high-frequency coefficients in recent studies [24–26] proposing approaches based on multiscale transforms, fusion selection rules suitable for these approaches have also been developed.

As previously stated, EDOF has many literature studies and is one of the most preferred strategies in the microscopic system to produce the image in which the full area of the specimen is focused. However, this research field still contains some crucial shortcomings. The shortcomings of the literature studies that presented EDOF approach can be summarized as follows:

1. Wavefront coding-based approaches can provide great precision and real-time performance, but they have high computational costs and complexity and require additional equipment.
2. The literature includes so many studies which proposed various focus measurement operators and image fusion techniques [27–29]. Moreover, researchers have carried out many algorithms for image fusion, especially in other research areas such as medical imaging [30–32] and remote sensing [33, 34]. However, there are a limited number of image fusion-based studies for EDOF microscopy despite their lower cost and not requiring additional equipment.
3. Compared to conventional approaches (Variance, Tenengrad), recent approaches based on CDWT, DCT, and NSST offer more precise focus degree for EDOF microscope. Literature studies, however, reveal that these approaches are unable to deal with various constraints, such as low precise characterization of curves and edges in images, and higher execution time.
4. There is no multi-focus image data set that is used to comprehensively analyze the performance of EDOF approaches.
5. To ease the limitations of traditional EDOF approaches (gradient, laplacian, and statistics-based), the research-

ers typically adopt a pre- or post-processing methodology rather than proposing a completely new focus measurement operator.
6. The majority of image fusion-based EDOF approaches perform adequately in areas with dense texture, but they struggle in areas with loud or weak texture. They are not specimen-free, and their performances vary depending on the specimen and microscope.
7. The sizes of the feature matrices generated by the multi-scale transform-based (discrete wavelet transform and discrete curvelet transform) EDOF approaches are different from the sizes of the input images (multi-focus images). As a result, focus details of input images are not fully recovered.
8. Convolutional neural networks (CNN) and deep learning have evolved significantly and rapidly in the research fields such as image processing, computer vision, internet of things, and medical image analysis in recent years [35–39]. However, the literature only contains a few numbers of CNN-based EDOF approaches. This, according to our literature review, is because there isn't an adequate amount of data set to construct CNN-based EDOF approaches.

Main Purpose and Contributions of This Study

In order to overcome the limitations of the literature studies presenting EDOF microscope, the purpose of this study is to develop more accurate and specimen-free EDOF microscope approach which produces an image in which the full area of the specimen is focused by using a collection consisting of the multi-focus images. The primary contributions of the suggested study are as follows:

1. Our review of the literature indicates that this is the first study to propose a deep learning-based EDOF microscope approach.
2. Contrary to literature approaches with various constraints such as low precise characterization of curves and edges in images, higher execution time and performance variation according to specimen and microscope (especially recent measurement operators based on Wavelet, Curvelet, 2D and 3D Steerable filters, NSST), this study provides more accurate and specimen-free EDOF microscope approach.
3. In order to provide comprehensive and specimen-free performance analysis of EDOF approaches, a novel multi-focus image data set is generated in this study, which is created using different specimen and magnification objective.
4. To produce an image in which the entire area of the specimen is focused, the recommended approach does not require any pre- or post-processing techniques.
5. The proposed EDOF approach acquires the pixel's focus degrees using deep features, which can produce more sharp variation regarding images, in contrast to literature studies employing solely the gray levels of the multi-focus images.
6. Since the sizes of the coefficient representations (lowpass and highpass coefficients) are different from the sizes of input images (multi-focus images) in the earlier studies proposing multi-scale transform (CDWT and DCT) based approach, they are resized to provide one to one correspondence between the pixels. This makes it impossible to extract critical focus details from the images. This issue is resolved in this study by utilizing deep feature matrices that are the same size as the input images.

The rest of this study has been designed as follows: The "Methodology'' section includes two subsections, briefly introducing novel multi-focus image data set, the structure, and an overview of the deep learning model, which forms the foundation for the EDOF microscope approach. The experimental results and discussion are presented in the "Experiments and Discussion'' section. Finally, the "Conclusion'' section summarizes the conclusion.

Methodology

This study is built on two main objectives: (1) Generating a novel multi-focus image data set and (2) proposing a deep learning-based EDOF approach. These subsections of study can be described as follows:

Multi-Focus Image Data Set

In order to provide comprehensive and specimen-free performance analysis of EDOF approaches, a novel multi-focus image data set including synthetic and real microscope image collections is generated in this study.

Synthetic Image Collections

Synthetic image collections are created using defocus simulation model generated by Pertuz et al. [8] (https://www.mathworks.com/matlabcentral/fileexchange/55095-defocus-simulation). This model simulates defocus in order to generate a multi-focus image collection. It operates by mapping an image (texture) to a depth map with a predetermined shape and simulating defocus for various focus points. Four different images are operated to simulate multi-focus image collections. Examples of multi-focus images from synthetic image collections — 1, 2, 3, and 4, details of which are outlined in Table 1, are shown in Fig. 2. The Synthetic Image Collection — 1 is created by mapping an image with

Table 1 Details of Synthetic Image Collections — 1, 2, 3, and 4

Collection	Number of images	Focus distance	Shape
Synthetic image	20	50–500 mm	Cos
Collection — 1	25	100–500 mm	Plane
	30	200–500 mm	Sphere
	35	200–400 mm	Cone
Synthetic image	20	50–250 mm	Cos
Collection — 2	25	100–300 mm	Plane
	30	200–500 mm	Sphere
	35	200–450 mm	Cone
Synthetic image	20	200–400 mm	Cos
Collection — 3	25	50–300 mm	Plane
	30	150–250 mm	Sphere
	35	50–450 mm	Cone
Synthetic image	20	100–300 mm	Cos
Collection — 4	25	50–300 mm	Plane
	30	30–300 mm	Sphere
	35	40–400 mm	Cone

a resolution of 256 × 256 and 3.3 mm focal length. This collection involves 20 images, which are acquired from 50 to 500 mm focus distance and with cos shape, 25 images, which are acquired from 100 to 500 mm focus distance and with plane shape, 30 images, which are acquired from 200 to 500 mm focus distance and with sphere shape, 35 images, which are acquired from 200 to 400 mm focus distance and with cone shape, respectively. The Synthetic Image Collection — 2 is created by mapping an image with 240 × 240-pixel size and 3.3 mm focal length. This collection involves 20 images, which are acquired at focus distances ranging from 50 to 250 mm and with cos shape, 25 images, which are acquired at focus distances ranging from 100 to 300 mm and with plane shape, 30 images, which are acquired at focus distances ranging from 200 to 500 mm and with sphere shape, 35 images, which are acquired at focus distances ranging from 200 to 450 mm and with cone shape, respectively. The Synthetic Image Collection — 3 is created by mapping an image with a resolution of 300 × 300 and 3.3 mm focal length. This collection involves 20 images, which are acquired from 200 to 400 mm focus distance and with cos shape, 25 images, which are acquired from 50 to 300 mm focus distance and with plane shape, 30 images, which are acquired from 150 to 250 mm focus distance and with sphere shape, 35 images, which are acquired from 50 to 450 mm focus distance and with cone shape, respectively. The Synthetic Image Collection — 4 is created by mapping an image with 256 × 256 pixel size and 3.3 mm focal length. This collection involves 20 images, which are acquired at focus distances ranging from 100 to 300 mm and with cos shape, 25 images, which are acquired at focus distances ranging from 50 to 300 mm and with plane shape, 30 images, which are acquired at focus distances ranging from 30 to 300 mm and with sphere shape, 35 images, which are acquired at focus distances ranging from 40 to 400 mm and with cone shape, respectively.

Microscope Image Collections

In addition to synthetic image collections, microscope image collections are created in this study. In order to create these collections, firstly 5 tissue specimens of mouse, which are heart, lung, liver, kidney, and intestine, stained with hematoxylin-eosin (HE), are prepared, and then multi-focus images are acquired scanning microscope stage. Examples of multi-focus images from microscope image collections — 1, 2, 3, 4, and 5, details of which are outlined in Table 2, are shown in Fig. 3. ×10 and ×40 magnification objectives are utilized in Zeiss Primo microscope. The multi-focus images of all collections are captured using Zeiss Axiocam microscope camera. They have different pixel sizes which are 1920 × 1080, 1420 × 760, 1450 × 800, 1050 × 600, and 1300 × 640, and saved in PNG file format. The numbers of multi-focus images in microscope image collections are 29, 35, 21, 36, 31, 22, 33, 40, 18, and 32.

Deep Learning Based Approach for EDOF (DL-EDOF)

This study presents a more accurate and specimen-free EDOF microscope approach based on unsupervised deep learning to produce an image in which the full area of the specimen is focused. This approach is performed in two main stages, training and combining. In the training stage, an auto-encoder model is designed to gather high-dimensional characteristics of input images (multi-focus images). In the combining stage, the pixel's focus values are calculated using deep characteristics, and an image in which the full area of the specimen is focused is produced using a collection of multi-focus images. These stages can be described as follows:

Training Stage

In the training stage, an auto-encoder model is constructed to acquire high-dimensional characteristics of multi-focus images. The structure of the auto-encoder model constructed in the training stage is shown in Fig. 4. The constructed auto-encoder model is trained at this stage, and the model's trainable parameters are fixed. As illustrated in Fig. 4, the auto-encoder model contains two primary parts; encoder and decoder.

1. Encoder: Capturing the global attributes of the pixels is the primary priority of this part. The image is taken as the input for this part after being scaled down to 256 × 256 and

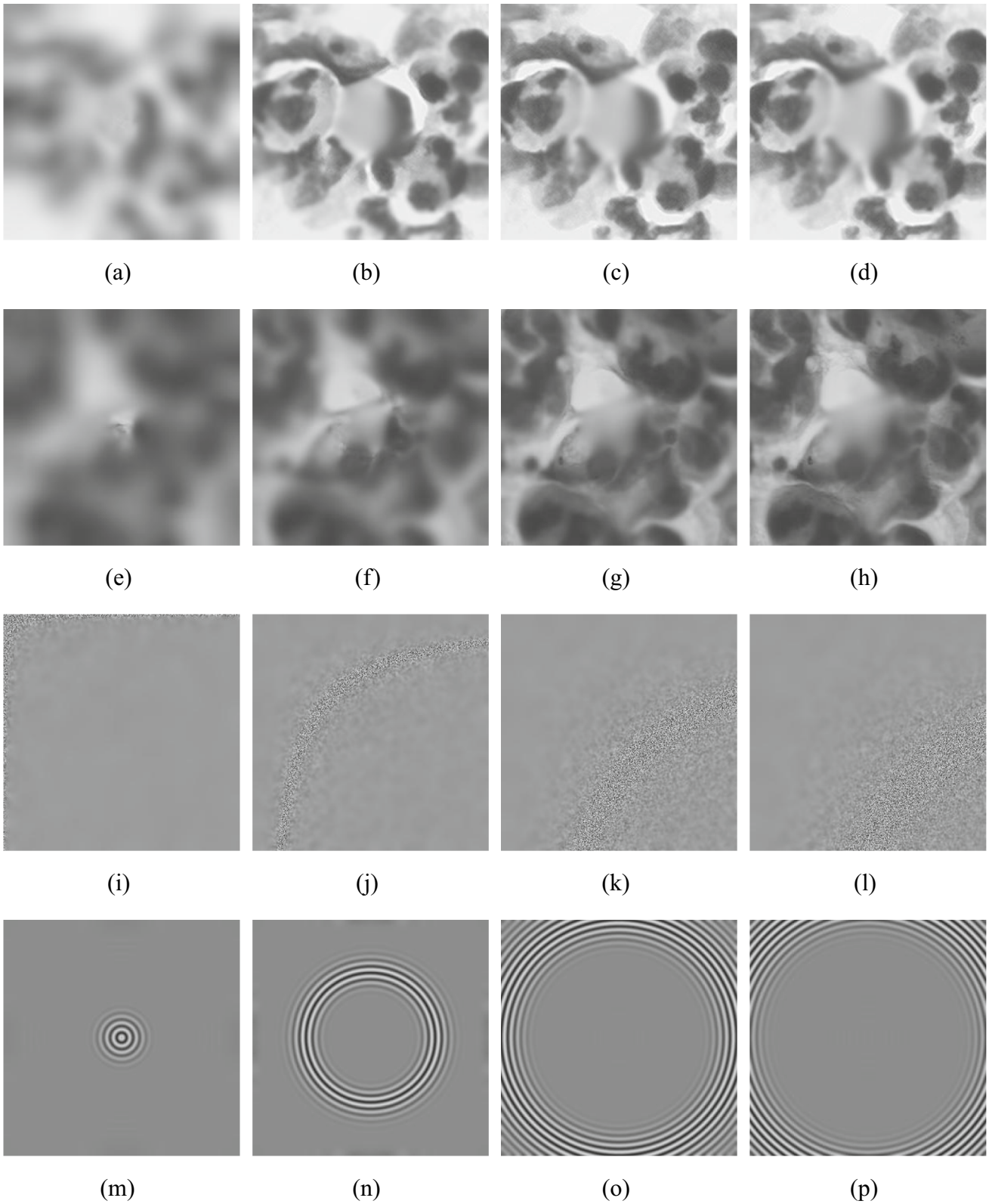

Fig. 2 Examples of multi-focus images from synthetic image collections — 1 (**a**, **b**, **c**, **d**); 2 (**e**, **f**, **g**, **h**); 3 (**i**, **j**, **k**, **l**); 4 (**m**, **n**, **o**, **p**)

Table 2 Details of Microscope Image Collections — 1, 2, 3, 4, and 5

Collection	Tissue	Image size	Objective	Number of images
Microscope image	Heart	1920 × 1080	10×	29
Collection — 1	Heart	1920 × 1080	40×	35
Microscope image	Lung	1420 × 760	10×	21
Collection — 2	Lung	1420 × 760	40×	36
Microscope image	Liver	1450 × 800	10×	31
Collection — 3	Liver	1450 × 800	40×	22
Microscope image	Kidney	1050 × 600	10×	33
Collection — 4	Kidney	1050 × 600	40×	40
Microscope image	Intestine	1300 × 640	10×	18
Collection — 5	Intestine	1300 × 640	40×	32

turned into gray scale. As output, 64 deep feature matrices (256 × 256) in total are generated. There are five sections which contain convolutional and spatial squeeze and channel excitation (cSE) blocks, whose outputs are linked to another. The convolutional block consists of 1 convolutional (Conv 2D) with 3 × 3 kernel size and 1 stride, 1 Relu, and 1 batch normalization layers. Due to claims in the literature studies that smaller kernel sizes are more efficient for retrieving relevant information from the images, the kernel sizes of all convolutional layers in all convolutional blocks are set to 3 × 3. As shown in Fig. 4, the kernel numbers of the convolution blocks are 16, 16, 32, 48, and 64, respectively. The objective of the encoder part is to produce deep feature matrices with the same size as the input image, so distinct layers like pooling are not used to precisely rebuild the image. In addition to convolutional blocks, cSE blocks are used in the encoder part to increase the generalizability and strength of the deep features. The cSE blocks include 1 average pooling and 2 dense layers. These blocks encode the global spatial data into a vector using a global average pooling layer, which passes through two dense layers to create a new vector.

2. Decoder: This part recreates the input image (256 × 256) using the attributes of the pixels, which are captured in the encoder phase. In this part, the deep feature matrices (256 × 256 × 64) are taken as input, and an image with 256 × 256 size is produced as output. There are four convolutional blocks, which consist of 1 convolutional with 3 × 3 kernel size and 1 stride, 1 relu, and 1 batch normalization layers. As given in Fig. 4, the kernel numbers of the convolution blocks are 64, 48, 32, and 16, respectively.

Combining Stage

The combining stage creates an image in which the full area of the specimen is focused using a collection of multi-focus images. Figure 5 shows the schematic diagram of the combining stage. As shown in Fig. 5, this stage consists of four fundamental phases: (1) producing a collection of multi-focus images, (2) generating deep feature matrices, (3) calculating focus values of pixels, and (4) selecting pixels with maximum focus values. These phases are explained as follows:

1. Producing a collection of multi-focus images: In the first phase, a collection of multi-focus images $(I_1(m,n), I_2(m,n), I_3(m,n), \ldots, I_K(m,n))$ are produced, where the image indices are represented by K, the pixel coordinates are m and n.
2. Generating deep feature matrices: The second phase utilizes the parameters of the auto-encoder model trained in the previous stage (training stage) to obtain a total of 64 deep feature matrices for each multi-focus image.
3. Calculating focus values of pixels: The EDOF microscope approaches necessitate pixel-to-pixel alignment between multi-focus images. Since the previous studies use the multi-scale transform (DCWT, DCT), where sizes of coefficient representations (lowpass and highpass coefficients) are not the same as the source images, the representations of multi-focus images are resized to supply pixel-to-pixel alignment. This makes it impossible to extract significant characteristic details from the images. This study uses deep feature matrices with the same sizes as the input images to address this issue. In the third phase, the focus measures $(FM_1(m,n), FM_2(m,n), FM_3(m,n), \ldots, FM_K(m,n))$ of multi-focus images are calculated with focus fusion rule. The focus fusion rule selects the highest pixel's focus values on the deep feature matrices.
4. Selecting pixels with maximum focus values: In the fourth phase, the fusion selection rule, which searches the pixels with the maximum focus value, is utilized in order to create an image ($CI(m,n)$) in which the full area of the specimen is focused.

$$CI(m,n) = argmax(FM(m,n)) \tag{1}$$

In Eq. (1), $CI(m, n)$ represents the image in which the full area of the specimen is focused, m and n are the pixel locations of image.

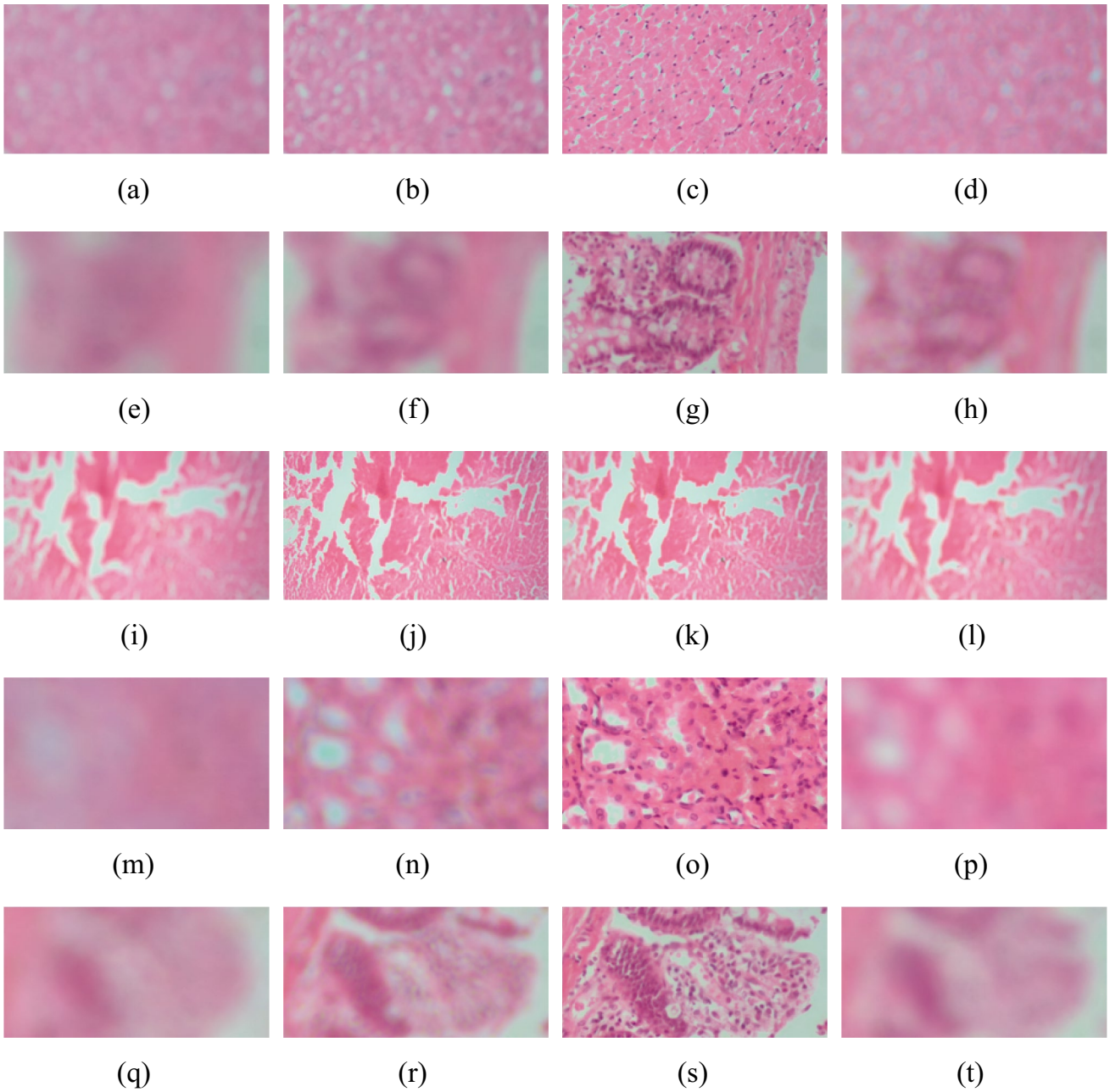

Fig. 3 Examples of multi-focus images from Microscope Image Collections — 1 (**a**, **b**, **c**, **d**); 2 (**e**, **f**, **g**, **h**); 3 (**i**, **j**, **k**, **l**); 4 (**m**, **n**, **o**, **p**); 5 (**q**, **r**, **s**, **t**)

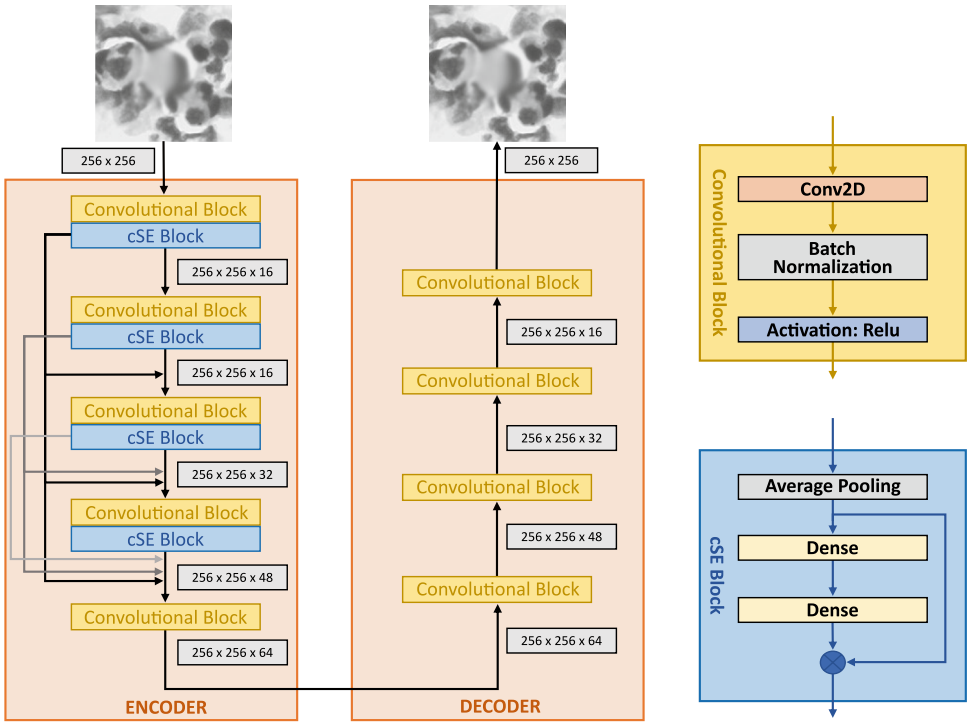

Fig. 4 Structure of auto-encoder model constructed in training stage

Experiments and Discussion

Software and Device Settings

The deep learning framework Pytorch is employed to experiment with the proposed EDOF microscope approach. The training and combining stages are compiled in the Pytorch environment. The programming language is Python 3.9 based on the Windows system with Miniconda 3 package management software. For implementation of EDOF microscope approaches, this study uses a hardware configuration that includes a PC with an Intel Core i7-9750 processor operating at 2.60 GHz, 32 GB of RAM, and an NVIDIA GeForce RTX 3060 GPU with 12 GB of GPU VRAM.

Performance Analysis Metrics

The synthetic image collections include a reference image used to evaluate the efficiency of EDOF microscope approaches. In this study, therefore, performance analysis metrics with requiring a reference image are preferred to identify which approach can extract more essential details from the multi-focus images for the synthetic collections. These performance analysis metrics are as follows:

- Root Mean Square Error (RMSE):
  RMSE identifies the similarity between the image created with EDOF microscope approach and the reference image. The RMSE value of the image generated with the ideal approach is expected to be smaller than the other approaches. The calculation of RMSE is given by

$$RMSE = \sqrt{\frac{1}{K * L}\sum_{i=1}^{K}\sum_{j=1}^{L}(RI_{i,j} - CI_{i,j})^2} \tag{2}$$

  where CI and RI are the images created with the EDOF microscope approach and reference image, K and L refer to the sizes of the images.
- Peak Signal to Noise Ratio (PSNR):
  PSNR is a measure which represents the relation between the image created with EDOF microscope approach and the reference image. The PSNR value of the image generated with the ideal approach is expected to be higher than the other approaches. PSNR measure is calculated by

$$PSNR = 20 * \log_{10}\left(\frac{H^2}{\sqrt{\frac{1}{K*L}\sum_{i=1}^{K}\sum_{j=1}^{L}(RI_{i,j} - CI_{i,j})^2}}\right) \tag{3}$$

  where CI and RI are the image created with EDOF microscope approach and reference image, H is the highest value in the CI, K, and L refer to the sizes of the images.
- Universal Quality Index (UQI):
  UQI is utilized to measure the disturbance between the image created with EDOF microscope approach

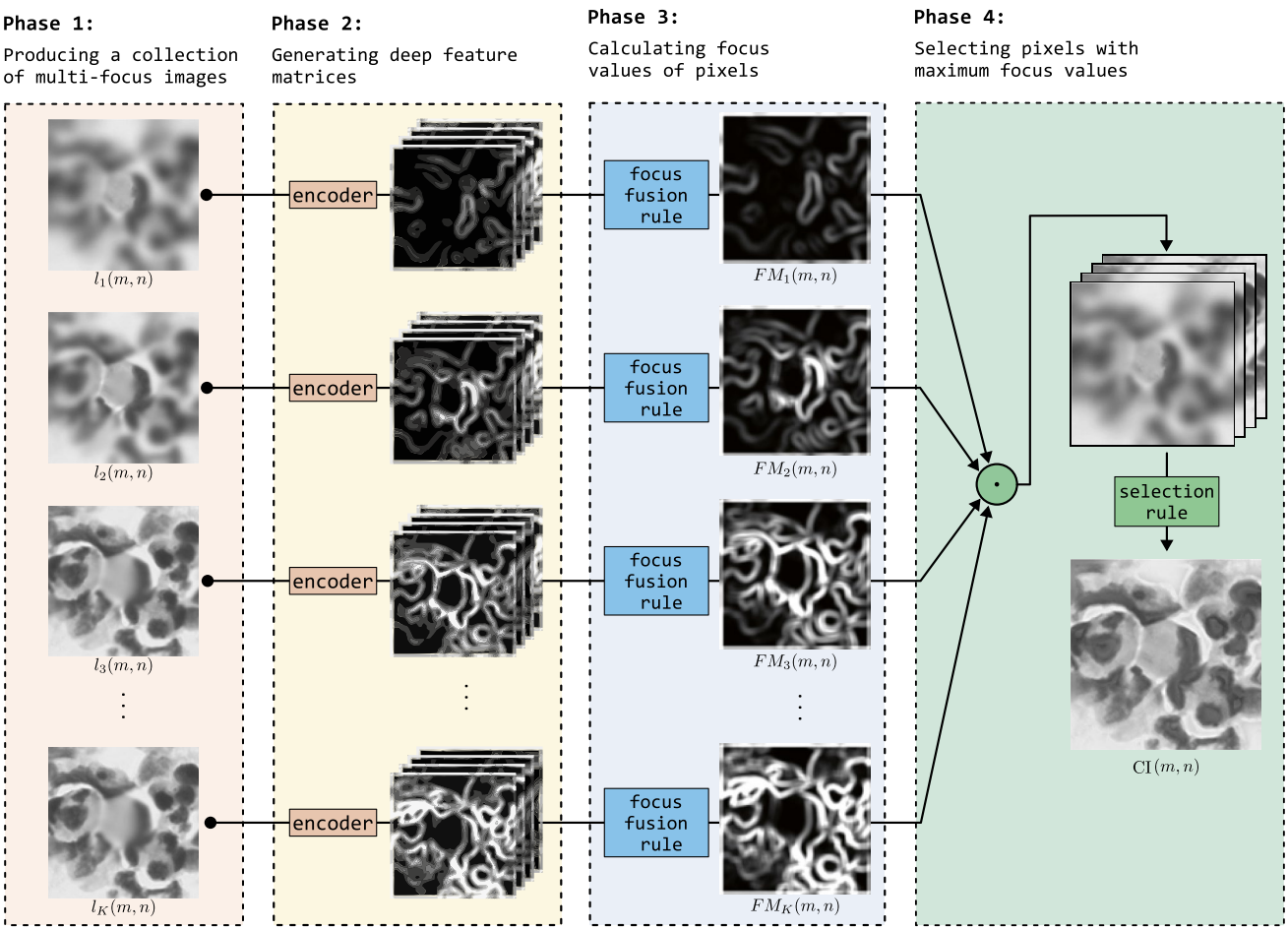

Fig. 5 Schematic diagram of combining stage: (1) producing a collection of multi-focus images, (2) generating deep feature matrices, (3) calculating focus values of pixels, and (4) selecting pixels with maximum focus values

and the reference image. The fact that the UQI value of the image is close to 1 indicates that the approach is ideal. UQI measure is computed by

$$UQI = \frac{4\sigma_{RI,CI}\bar{RI}\,\bar{CI}}{(\sigma_{RI}^2 + \sigma_{CI}^2)(\bar{RI}^{\,2} + \bar{CI}^{\,2})} \tag{4}$$

where $\bar{RI}$ and $\bar{CI}$ are the means of the values on the reference image and image created with EDOF microscope approach, $\sigma_{RI,CI}$, σ_{RI}, and σ_{CI} represent the covariance and variances of the values on the reference image and image created with EDOF microscope approach.

- Correlation Coefficient (CC):

  CC gives a value about the relation between the image created with EDOF microscope approach and the reference image. The CC value of the image generated with ideal approach is expected to be higher than the other approaches. The computation of CC is given by

$$CC = \frac{\sum_i \sum_j (RI_{i,j} - \bar{RI})(CI_{i,j} - \bar{CI})}{\sqrt{\left(\sum_i \sum_j (RI_{i,j} - \bar{RI})\right)^2 \left(\sum_i \sum_j (CI_{i,j} - \bar{CI})\right)^2}} \tag{5}$$

  where CI and RI are the image created with EDOF microscope approach and reference image, $\bar{RI}$ and $\bar{CI}$ refer to the means of the values on the reference image and image created with EDOF microscope approach.

In addition to synthetic image collections, microscope image collections are used to assess the efficiencies of EDOF microscope approaches. However, the microscopic system does not have an image which can be recognized as a reference (ideal), so performance analysis metrics without requiring a reference image are preferred to identify which approach can extract the more critical focus data from the multi-focus images. These performance analysis metrics are as follows:

Table 3 Objective results of performance analysis metrics calculated with different EDOF approaches for Synthetic Image Collections — 1 and 2

	Category	Approach	RMSE	PSNR	UQI	CC
Synthetic Image Collection — 1	Gradient	Gaussian Derivative	3.7114	29.0398	0.9864	0.9869
		Tenengrad	3.6951	28.9906	0.9863	0.9868
		Gradient Energy	3.1612	30.5330	0.9905	0.9907
	Laplacian	Energy of Laplacian	3.1495	32.3775	0.9869	0.9869
		Multi-Directional Modified Laplacian	3.2278	31.7333	0.9864	0.9865
		Laplacian in 3D	3.2278	31.7333	0.9864	0.9865
	Wavelet Transform	Sum of Wavelet Coefficient	3.8388	30.8237	0.9816	0.9837
		3D Wavelet Coefficient	3.8328	30.9098	0.9816	0.9837
		Variance of Wavelet Coefficient	3.8444	30.9199	0.9814	0.9835
	Statistics	Chebysev Moments	4.2931	28.6330	0.9753	0.9778
		Eigen Values	4.2052	29.3913	0.9805	0.9825
		Variance	4.2889	29.2487	0.9801	0.9821
	Cosine Transform	DCT Reduced Energy Ratio	4.5102	28.7504	0.9783	0.9806
		DCT Energy Ratio	4.2273	29.3360	0.9802	0.9822
	Others	Spatial Frequency	4.0595	29.7906	0.9816	0.9836
		Discrete Curvelet Transform	4.0472	29.0112	0.9812	0.9850
		Brenner	4.2516	29.4540	0.9804	0.9825
		2D Steerable Filter	4.4938	28.8649	0.9788	0.9811
		Gabor Features	4.2006	29.4866	0.9808	0.9828
		Non-Subsampled Shearlet Transform	3.8216	31.0235	0.9843	0.9852
	Proposed	**DL-EDOF**	**2.9065**	**34.1112**	**0.9943**	**0.9949**
Synthetic Image Collection — 2	Gradient	Gaussian Derivative	3.8153	31.0903	0.9820	0.9834
		Tenengrad	3.7982	31.1758	0.9824	0.9837
		Gradient Energy	3.7380	31.2575	0.9827	0.9840
	Laplacian	Energy of Laplacian	3.6639	31.6613	0.9836	0.9849
		Multi-Directional Modified Laplacian	3.6786	31.6039	0.9835	0.9848
		Laplacian in 3D	3.6786	31.6039	0.9835	0.9848
	Wavelet Transform	Sum of Wavelet Coefficient	3.7494	31.4522	0.9829	0.9843
		3D Wavelet Coefficient	3.7317	31.6303	0.9834	0.9847
		Variance of Wavelet Coefficient	3.7456	31.5159	0.9831	0.9845
	Statistics	Chebysev Moments	4.5220	29.6265	0.9733	0.9757
		Eigen Values	3.7337	31.4724	0.9834	0.9846
		Variance	3.7989	31.2096	0.9825	0.9838
	Cosine Transform	DCT Reduced Energy Ratio	3.8924	31.0858	0.9822	0.9835
		DCT Energy Ratio	3.7393	31.5071	0.9835	0.9847
	Others	Spatial Frequency	3.7382	31.2581	0.9827	0.9840
		Discrete Curvelet Transform	3.7411	31.2103	0.9826	0.9837
		Brenner	3.8410	31.1905	0.9823	0.9837
		2D Steerable Filter	4.0198	30.8687	0.9811	0.9826
		Gabor Features	3.7830	31.1159	0.9822	0.9835
		Non-Subsampled Shearlet Transform	3.6620	31.6105	0.9831	0.9840
	Proposed	**DL-EDOF**	**3.3510**	**33.1590**	**0.9937**	**0.9915**

Table 4 Objective results of performance analysis metrics calculated with different EDOF approaches for Synthetic Image Collections — 3 and 4

	Category	Approach	RMSE	PSNR	UQI	CC
Synthetic Image Collection — 3	Gradient	Gaussian Derivative	6.5183	26.5348	0.9388	0.9396
		Tenengrad	6.5215	26.5310	0.9387	0.9396
		Gradient Energy	6.5159	26.5083	0.9386	0.9395
	Laplacian	Energy of Laplacian	6.5164	26.5276	0.9388	0.9396
		Multi-Directional Modified Laplacian	6.5133	26.5408	0.9388	0.9397
		Laplacian in 3D	6.5133	26.5408	0.9388	0.9397
	Wavelet Transform	Sum of Wavelet Coefficient	6.5124	26.5560	0.9390	0.9398
		3D Wavelet Coefficient	6.5136	26.5425	0.9389	0.9398
		Variance of Wavelet Coefficient	6.5305	26.4679	0.9383	0.9391
	Statistics	Chebysev Moments	6.5965	26.1711	0.9350	0.9358
		Eigen Values	6.4985	26.5706	0.9392	0.9401
		Variance	6.4991	26.5698	0.9393	0.9401
	Cosine Transform	DCT Reduced Energy Ratio	6.6309	25.3599	0.9287	0.9295
		DCT Energy Ratio	6.4995	26.5203	0.9364	0.9373
	Others	Spatial Frequency	6.5158	26.5083	0.9386	0.9395
		Discrete Curvelet Transform	6.5163	26.5213	0.9386	0.9394
		Brenner	6.5205	26.4919	0.9385	0.9393
		2D Steerable Filter	6.5170	26.5416	0.9388	0.9397
		Gabor Features	6.5080	26.5632	0.9391	0.9399
		Non-Subsampled Shearlet Transform	6.5093	26.5428	0.9390	0.9399
	Proposed	**DL-EDOF**	**6.3088**	**26.9204**	**0.9423**	**0.9479**
Synthetic Image Collection — 4	Gradient	Gaussian Derivative	3.6911	33.4429	0.9901	0.9909
		Tenengrad	3.6211	33.3870	0.9901	0.9909
		Gradient Energy	3.8514	29.3629	0.9856	0.9866
	Laplacian	Energy of Laplacian	3.6338	33.4435	0.9901	0.9909
		Multi-Directional Modified Laplacian	3.6454	33.4580	0.9900	0.9909
		Laplacian in 3D	3.6454	33.4580	0.9900	0.9909
	Wavelet Transform	Sum of Wavelet Coefficient	4.6806	29.7166	0.9850	0.9875
		3D Wavelet Coefficient	4.5997	28.6020	0.9829	0.9859
		Variance of Wavelet Coefficient	5.0435	28.2693	0.9815	0.9849
	Statistics	Chebysev Moments	3.6884	34.1618	0.9709	0.9893
		Eigen Values	3.6150	33.2447	0.9900	0.9909
		Variance	3.6213	33.3900	0.9901	0.9910
	Cosine Transform	DCT Reduced Energy Ratio	3.8924	31.0858	0.9822	0.9835
		DCT Energy Ratio	3.6218	33.1186	0.9899	0.9908
	Others	Spatial Frequency	3.8514	29.3630	0.9856	0.9866
		Discrete Curvelet Transform	3.7498	32.9983	0.9874	0.9878
		Brenner	3.6976	33.1473	0.9898	0.9907
		2D Steerable Filter	3.6237	33.4801	0.9901	0.9910
		Gabor Features	3.6455	33.2743	0.9899	0.9908
		Non-Subsampled Shearlet Transform	3.6650	33.3316	0.9896	0.9882
	Proposed	**DL-EDOF**	**3.0195**	**36.1254**	**0.9940**	**0.9963**

Table 5 Objective results of performance analysis metrics calculated with different EDOF approaches for Microscope Image Collections — 1 and 2

	Category	Approach	PIQE	BRISQUE	UQIN	NIQE
Microscope Image Collection — 1	Gradient	Gaussian Derivative	43.8854	29.9203	0.0907	7.8787
		Tenengrad	43.3822	26.9518	0.0905	7.9228
		Gradient Energy	42.3390	25.9733	0.0912	7.9091
	Laplacian	Energy of Laplacian	40.2429	26.5040	0.0932	7.7973
		Multi-Directional Modified Laplacian	40.2376	25.8902	0.0937	7.7025
		Laplacian in 3D	40.2376	25.8902	0.0937	7.7025
	Wavelet	Sum of Wavelet Coefficient	40.6387	26.3381	0.0945	7.9008
		3D Wavelet Coefficient	41.4758	26.2626	0.0946	7.8871
		Variance of Wavelet Coefficient	41.9975	26.7113	0.0956	7.7521
	Statistics	Chebysev Moments	48.2492	34.3237	0.0890	9.9355
		Eigen Values	46.5549	31.3669	0.0901	8.7034
		Variance	46.3383	30.9234	0.0904	8.7136
	Cosine Transform	DCT Reduced Energy Ratio	48.3699	35.4852	0.0897	8.7615
		DCT Energy Ratio	49.1536	36.3570	0.0891	8.6189
	Others	Spatial Frequency	42.6601	25.9663	0.0912	7.9194
		Discrete Curvelet Transform	42.5566	25.4133	0.0910	7.9052
		Brenner	42.5188	25.8067	0.0909	7.9088
		2D Steerable Filter	43.9716	26.7348	0.0911	7.9941
		Gabor Features	42.7622	25.4067	0.0913	8.0596
		Non-Subsampled Shearlet Transform	41.9987	25.1112	0.0911	7.9114
	Proposed	**DL-EDOF**	**38.5842**	**22.1101**	**0.1070**	**6.5082**
Microscope Image Collection — 2	Gradient	Gaussian Derivative	58.0470	38.0676	0.3172	8.9487
		Tenengrad	56.9672	37.5640	0.3170	8.9006
		Gradient Energy	56.2258	35.5170	0.3166	8.0451
	Laplacian	Energy of Laplacian	55.3230	34.2490	0.3252	7.6036
		Multi-Directional Modified Laplacian	55.2384	34.5742	0.3258	7.6252
		Laplacian in 3D	55.2384	34.5742	0.3258	7.6252
	Wavelet	Sum of Wavelet Coefficient	55.6836	34.5360	0.3059	7.6594
		3D Wavelet Coefficient	57.4970	37.3378	0.3137	7.7251
		Variance of Wavelet Coefficient	56.1968	36.9485	0.3157	7.6534
	Statistics	Chebysev Moments	59.8695	39.2960	0.2984	8.7977
		Eigen Values	59.7732	38.6014	0.2976	8.6570
		Variance	59.3599	38.4999	0.2971	8.6893
	Cosine Transform	DCT Reduced Energy Ratio	61.6081	40.6963	0.2975	8.5678
		DCT Energy Ratio	61.9042	40.7851	0.2973	8.5868
	Others	Spatial Frequency	56.2897	35.5393	0.3066	8.0541
		Discrete Curvelet Transform	56.1122	36.7983	0.3079	8.7751
		Brenner	56.3670	37.2696	0.3074	8.4238
		2D Steerable Filter	57.4117	38.0146	0.3079	8.8554
		Gabor Features	56.7000	37.2007	0.3073	8.1667
		Non-Subsampled Shearlet Transform	56.1212	37.1112	0.3075	8.3315
	Proposed	**DL-EDOF**	**52.5115**	**31.1567**	**0.3512**	**6.6673**

Table 6 Objective results of performance analysis metrics calculated with different EDOF approaches for Microscope Image Collections — 3, 4, and 5

	Category	Approach	PIQE	BRISQUE	UQIN	NIQE
Microscope Image Collection — 3	Gradient	Gaussian Derivative	45.3449	36.1457	0.0772	9.1115
		Tenengrad	44.2059	34.1975	0.0764	9.1680
		Gradient Energy	42.7843	34.7746	0.0772	9.0499
	Laplacian	Energy of Laplacian	40.6009	31.9745	0.0827	8.4256
		Multi-Directional Modified Laplacian	40.1350	31.9507	0.0820	8.5498
		Laplacian in 3D	40.1350	31.9507	0.0820	8.5498
	Wavelet	Sum of Wavelet Coefficient	41.0996	32.0819	0.0820	8.5753
		3D Wavelet Coefficient	41.1271	32.6248	0.0824	8.5132
		Variance of Wavelet Coefficient	41.9641	32.8583	0.0820	8.6347
	Statistics	Chebysev Moments	46.1159	41.3721	0.0763	10.1118
		Eigen Values	46.5531	41.2237	0.0760	9.0023
		Variance	46.9587	41.3305	0.0763	9.0464
	Cosine Transform	DCT Reduced Energy Ratio	49.1429	42.9862	0.0677	9.0782
		DCT Energy Ratio	49.2832	42.2644	0.0665	9.9805
	Others	Spatial Frequency	42.8804	33.7655	0.0773	9.0544
		Discrete Curvelet Transform	43.1184	34.5431	0.0785	9.2116
		Brenner	42.5211	33.7996	0.0786	8.9858
		2D Steerable Filter	45.3372	36.4729	0.0783	9.0619
		Gabor Features	44.3160	35.8072	0.0773	9.1849
		Non-Subsampled Shearlet Transform	42.4187	33.6366	0.0783	9.0111
	Proposed	**DL-EDOF**	**37.1345**	**28.6539**	**0.1133**	**6.8428**
Microscope Image Collection — 4	Gradient	Gaussian Derivative	39.9068	31.7235	0.3097	9.2503
		Tenengrad	39.0832	31.6976	0.3095	9.2712
		Gradient Energy	38.9116	31.5637	0.3020	9.1601
	Laplacian	Energy of Laplacian	39.9188	32.1871	0.3001	9.4173
		Multi-Directional Modified Laplacian	40.2810	32.9989	0.3003	9.6972
		Laplacian in 3D	40.2810	32.9989	0.3003	9.6972
	Wavelet	Sum of Wavelet Coefficient	41.2965	33.0949	0.2985	9.7286
		3D Wavelet Coefficient	42.2010	33.6782	0.2899	9.8583
		Variance of Wavelet Coefficient	42.7061	33.9993	0.2944	9.8661
	Statistics	Chebysev Moments	43.0160	34.1192	0.2760	11.1352
		Eigen Values	42.0858	33.3484	0.2875	10.0985
		Variance	41.5063	33.1498	0.2984	10.1159
	Cosine Transform	DCT Reduced Energy Ratio	43.1085	33.8263	0.2976	10.2559
		DCT Energy Ratio	44.0799	33.4533	0.2866	10.7683
	Others	Spatial Frequency	38.6239	31.5718	0.3111	9.2825
		Discrete Curvelet Transform	38.6412	31.4015	0.2090	9.3117
		Brenner	39.3790	31.4953	0.3093	9.6092
		2D Steerable Filter	39.6625	31.3093	0.3114	9.5960
		Gabor Features	39.6504	31.5145	0.3093	9.3440
		Non-Subsampled Shearlet Transform	38.6712	31.6174	0.3093	9.4537
	Proposed	**DL-EDOF**	**36.0928**	**28.1104**	**0.3994**	**8.7598**
Microscope Image Collection — 5	Gradient	Gaussian Derivative	47.3765	26.8044	0.2930	5.9398
		Tenengrad	46.9377	25.0933	0.3028	5.8453
		Gradient Energy	46.3928	25.2728	0.3028	5.8459
	Laplacian	Energy of Laplacian	47.0531	27.5470	0.2830	5.9577
		Multi-Directional Modified Laplacian	47.0308	27.5838	0.2832	6.0023
		Laplacian in 3D	47.0308	27.5838	0.2832	6.0023
	Wavelet	Sum of Wavelet Coefficient	47.8079	27.5383	0.2836	5.9060

Table 6 (continued)

	Category	Approach	PIQE	BRISQUE	UQIN	NIQE
		3D Wavelet Coefficient	49.1856	28.2616	0.2731	6.8295
		Variance of Wavelet Coefficient	48.5639	28.5573	0.2737	6.4248
	Statistics	Chebysev Moments	48.4935	27.8313	0.2926	5.9676
		Eigen Values	48.9450	27.2044	0.2922	5.6102
		Variance	48.5285	27.0662	0.2925	5.6304
	Cosine Transform	DCT Reduced Energy Ratio	50.3244	29.2315	0.2625	6.5118
		DCT Energy Ratio	50.5508	29.1042	0.2620	6.4781
	Others	Spatial Frequency	46.4555	25.2250	0.2928	5.8508
		Discrete Curvelet Transform	46.4498	25.8781	0.2930	5.8311
		Brenner	46.4363	26.0051	0.2935	5.8322
		2D Steerable Filter	46.8675	26.4140	0.2935	5.8976
		Gabor Features	46.7445	27.2996	0.2930	5.8449
		Non-Subsampled Shearlet Transform	46.6863	25.7411	0.2931	5.8417
	Proposed	**DL-EDOF**	**44.1298**	**23.9155**	**0.3287**	**5.0133**

- Perception-based Image Quality Evaluator (PIQE):
  PIQE is an analysis metric which provides a value about the quality of the image created with EDOF microscope approach [40]. The PIQE value of the image generated with ideal approach is expected to be lower than the other approaches.
- Blind/Referenceless Image Spatial Quality Evaluator (BRISQUE):
  BRISQUE gives a measure about the quality score of the image created with EDOF microscope approach [41]. The BRISQUE value of the image generated with ideal approach is expected to be lower than the other approaches.
- Extension of Universal Quality Index for N Images (UQIN):
  UQIN is utilized to determine a value about data transferred from the multi-focus images to image created with EDOF microscope approach. The UQIN value of the image generated with ideal approach is expected to be higher than the other approaches. UQIN measure is computed by

$$UQIN(I_1, I_2, ..., I_N, CI) = \frac{1}{\mid T \mid} \sum_{w \epsilon T} \sum_{k=1}^{N} \lambda_{I_k}(w) x UQI(I_k, CI \mid w) \quad (6)$$

$$\lambda_{I_k} = \frac{Y(I_k \mid w)}{\sum_{k=1}^{N} Y(I_k \mid w)} \quad (7)$$

  where $(I_1, I_2, ..., I_N)$ and CI are the multi-focus images and image created with EDOF microscope approach, w represents the ROI that is subdivided region of image and $Y(I_k \mid w)$ is variance value of the ROI.
- Naturalness Image Quality Evaluator (NIQE):
  NIQE gives a value about quality score of the image created with EDOF microscope approach [42]. The NIQE value of the image generated with ideal approach is expected to be lower than the other approaches.

Experiments on Training Stage

An auto-encoder model, a description of which is provided in the "Methodology'' section, is supplied during the training stage to acquire the high-dimensional characteristics of the multi-focus images. Because our EDOF microscope approach is based on unsupervised deep learning, the auto-encoder model is trained with the MS-COCO data set - 2017 [43]. Trainable parameters of this model are fixed and applied to combine the multi-focus images in the second (combining) stage. The numbers of batch size and epochs are selected as 48 and 40, respectively. Each epoch employs 5000 and 118,287 images for training and validation of this stage. Each image is downscaled to 256×256 pixels and transformed into gray scale.

Objective and Subjective Analysis on Combining Stage

The focus measurement operator is performed by processing the pixel's neighborhood in the conventional EDOF microscope approaches based on image fusion to calculate the focus values. In the second phase (calculating pixel's focus values in the collection of multi-focus images) of these approaches, only gray levels of the multi-focus images are used. Contrary to literature studies proposing conventional EDOF microscope approaches, the proposed approach acquires the pixel's focus values from deep features.

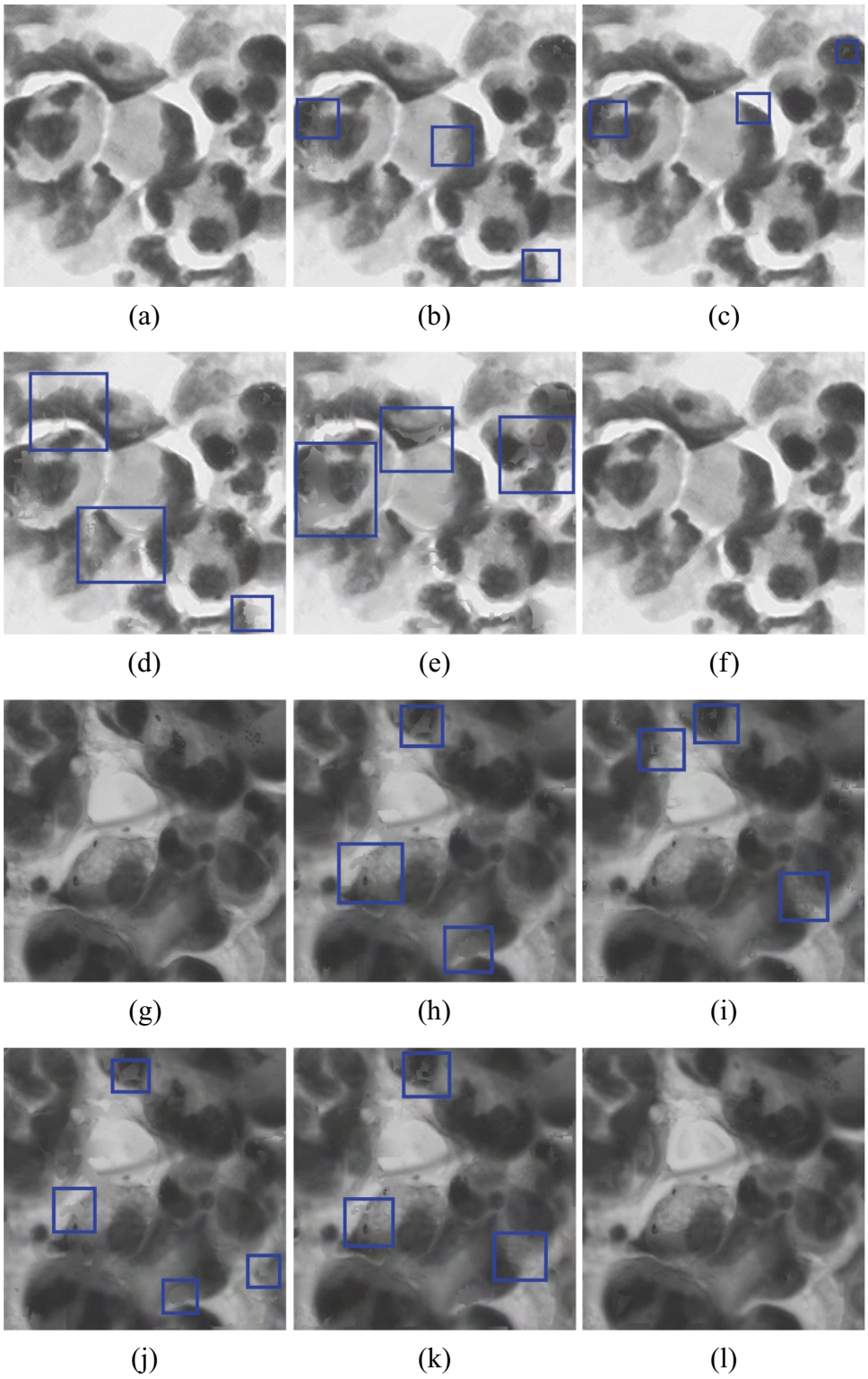

Fig. 6 Reference images (**a**–**g**), images created on Synthetic Image Collections — 1 and 2 with Tenengrad (**b**–**h**), Variance of Wavelet Coefficient (**c**–**i**), DCT Reduced Energy Ratio (**d**–**j**), Spatial Frequency (**e**–**k**), and proposed approach (DL - EDOF) (**f**–**l**)

A total of 20 approaches from 6 categories are applied to the image collections, details of which are listed in Tables 1 and 2, in order to assess the efficacy of our EDOF approach based on deep learning. While performance analysis metrics with requiring a reference image (RMSE, PSNR, UQI, and CC) are preferred to identify which EDOF approach can extract more essential details from the multi-focus images for the synthetic collections, performance analysis metrics without requiring a reference image (PIQE, BRISQE, UQIN, and NIQE) are preferred

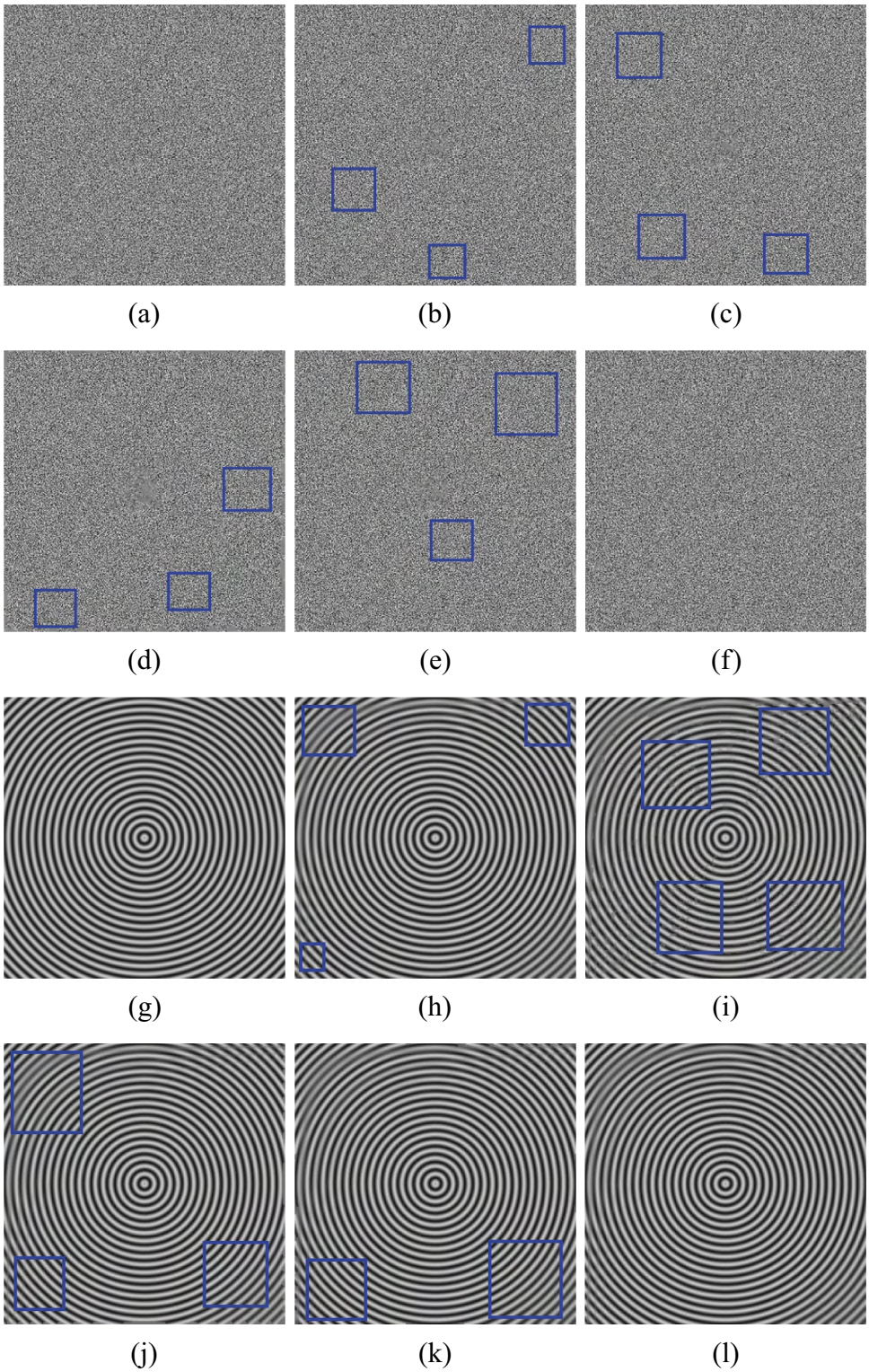

Fig. 7 Reference images (**a**–**g**), images created on Synthetic Image Collections — 3 and 4 with Tenengrad (**b**–**h**), Variance of Wavelet Coefficient (**c**–**i**), DCT Reduced Energy Ratio (**d**–**j**), Spatial Frequency (**e**–**k**), and proposed approach (DL - EDOF) (**f**–**l**)

for the microscope image collections. Tables 3, 4, 5, and 6 indicate the quantitative outcomes of performance analysis metrics calculated with different EDOF approaches for all image collections. As stated previously, an ideal EDOF approach is expected to produce an image with higher PSNR, UQI, CC, UQIN and lower RMSE, PIQE, BRISQUE, and NIQE. As shown in Tables 3, 4, 5, and 6, the performances of the EDOF approaches vary according to the data set and magnification of microscope objective. For example; Energy of Laplacian provides better

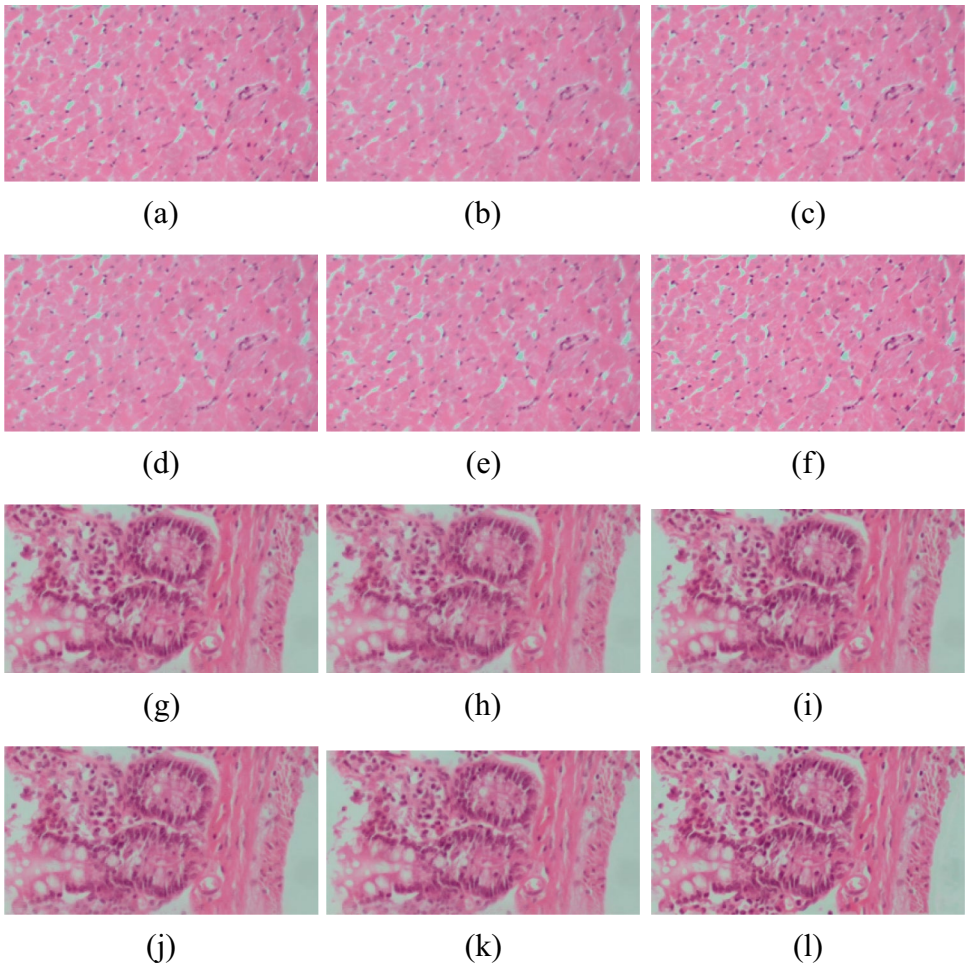

Fig. 8 Images created on Microscope Image Collections — 1 and 2 with Tenengrad (**a**–**g**), variance of wavelet coefficient (**b**–**h**), DCT Reduced Energy Ratio (**c**–**i**), Energy of Laplacian (**d**–**j**), Spatial Frequency (**e**–**k**), and proposed approach (DL - EDOF) (**f**–**l**)

performance for synthetic image collections — 1 and 2, while Eigen Values and Variance provide better performance for Synthetic Image Collection - 3. Moreover, this shortcoming of EDOF approaches is valid for microscope image collections. The results of performance analysis metrics indicate that the recommended approach (DL-EDOF) performs better than the most popular approaches for EDOF microscope in the literature. Contrary to literature approaches with various constraints such as low precise characterization of curves and edges in images and performance variation according to the specimen (especially recent measurement operators based on Wavelet, Curvelet, 2D Steerable filter, NSST), this study provides more accurate and specimen-free EDOF microscope approach. It is noteworthy that the EDOF approaches based on DCT and statistics provide the worst performance with the highest RMSE, PIQE, BRISQUE, NIQE, and the least PSNR, UQI, CC, and UQIN. The gray scales of multi-focus images are inappropriate for the EDOF approaches, as given in Tables 3, 4, 5, and 6. The proposed EDOF approach based on deep learning can provide adequate efficiency to transmit crucial details from images.

The references and images created with Tenengrad, Variance of Wavelet Coefficient, DCT Reduced Energy Ratio, Energy of Laplacian, Spatial Frequency, and proposed approach (DL - EDOF) on the synthetic and microscope image collections are shown in Figs. 6, 7, 8, and 9. By comparing reference images in Figs. 6a, g and 7a, g and the images generated with different EDOF approaches, it is noteworthy that our recommended approach has a greater performance. As shown in blue rectangles, patterns and blurriness that are not present in the input images (multi-focus images) are seen in the output images created with Tenengrad, Variance of Wavelet Coefficient, DCT Reduced Energy Ratio, Energy of Laplacian, Spatial Frequency. As illustrated in Figs. 6, 7, 8, and 9, the images created with proposed EDOF approach based on unsupervised deep learning have lowest levels of the blurring and noise and are the most similar to the reference images. The objective results, which demonstrate that unsupervised deep learning provides the optimum efficiency for all image collections in terms of RMSE, PSNR, UQI, CC, PIQE, BRISQUE, UQIN, and NIQE, are compatible with the subjective visuals in Figs. 6, 7, 8, and 9.

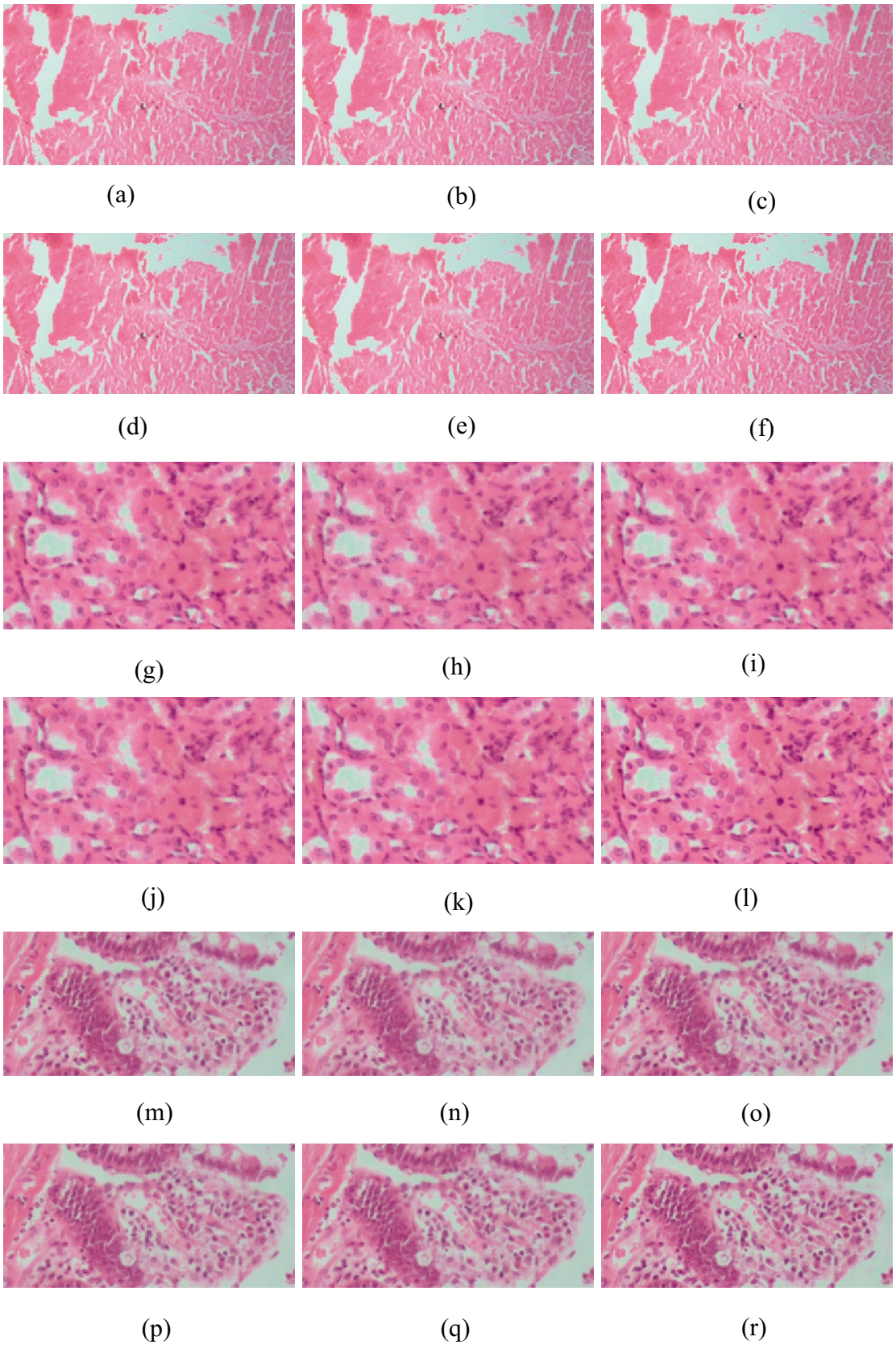

Fig. 9 Images created on microscope image collections — 3, 4, and 5 with Tenengrad (**a**–**g**–**m**), Variance of Wavelet Coefficient (**b**–**h**–**n**), DCT Reduced Energy Ratio (**c**–**i**–**o**), Energy of Laplacian (**d**–**j**–**p**), Spatial Frequency (**e**–**k**–**q**), and proposed approach (DL - EDOF) (**f**–**l**–**r**)

Conclusion

Overall Findings

In order to produce an image in which the full area of the specimen is focused, this study generates a novel multi-focus image data set and improves more accurate and specimen-free EDOF microscope approach. Our multi-focus image data set includes synthetic and real microscope image collections. While synthetic image collections are created using defocus simulation model, the tissue specimens of mouse, which are heart, lung, liver, kidney, and intestine, stained with HE are prepared for acquiring microscope image collections. Multi-focus image data set contains 9 image collections (4 synthetic and 5 microscope image collections) in total. The suggested EDOF microscope approach is divided into two stages: training and combining. In the training stage, we construct an auto-encoder model to acquire high-dimensional attributes of input images (multi-focus images). The combining stage produces an image in which the full area of the specimen is focused using a collection of multi-focus images.

Instead of proposing novel EDOF microscope approach in the literature, a pre- or post-processing algorithm is generally improved to combine image with higher accuracy and lower blurring. In this study, a novel EDOF approach based on unsupervised deep learning is proposed. In contrast to studies in the literature, our suggested approach offers better focus representation and higher performance. It has minimal computational costs and complexity because no pre- or post-processing algorithm is needed. Moreover, the suggested EDOF approach acquires the pixel's focus values from deep features, in contrast to previous studies employing only original images, which can provide more sharp variation regarding images.

Our proposed EDOF approach is evaluated theoretically and practically using a data set comprising of synthetic and real microscope image collections. To investigate which EDOF microscope approach can extract more vital characteristics of multi-focus images for synthetic image collections, performance analysis metrics with requiring a reference are used, which are RMSE, PSNR, UQI, and CC. Image created with a higher performance EDOF approach is expected to have lower RMSE and higher PSNR, UQI, and CC values. The results of these performance analysis metrics for the synthetic image collections show that our suggested EDOF approach is more effective than the other approaches because it has the highest values of PSNR, UQI, and CC and the lowest values of RMSE. Also, the visual findings indicate that the images produced using the proposed approach's unsupervised deep learning model have the least degree of blurring and noise, and are the most similar to the reference images. On the other hand, in order to investigate which EDOF microscope approach can extract more vital characteristics of multi-focus images for microscope image collections, performance analysis metrics without requiring a reference are used, which are PIQE, BRISQUE, UQIN, and NIQE. Image created with a higher performance EDOF approach is expected to have lower PIQE, BRISQUE, NIQE, and higher UQIN values. It is evident that our suggested approach, which has lower PIQE, BRISQUE, NIQE values, and higher UQIN values, performs better than other literature operators.

Current Constraints

As mentioned in the "Main Purpose and Contributions of This Study'' section, our study has many contributions for EDOF microscope, but there are some constraints in the developed approach. These constraints can be summarized as follows:

1. For implementation of EDOF microscope approaches, this study uses a hardware configuration that includes a PC with an Intel Core i7-9750 processor operating at 2.60 GHz, 32 GB of RAM, and an NVIDIA GeForce RTX 3060 GPU with 12 GB of GPU VRAM. In comparison to prior studies using deep learning and CNN-based techniques in image processing, computer vision, and medical imaging analysis, our GPU has significantly less memory. To minimize this hardware configuration constraint, we optimize GPU consumption by reducing the input image dimension to 256×256.
2. As previously stated, this is the first study to offer an EDOF microscope approach for acquiring pixel focus degrees utilizing deep features. In contrast to previous studies improving deep learning and CNN-based image processing techniques, we created a basic auto-encoder model for obtaining high-dimensional attributes from multi-focus images (EDOF microscope). This model is solely composed of convolutional and cSE blocks.

Future Works

As mentioned in the "Experiments and Discussion'' section, the success of the proposed EDOF microscope approach has been proven both numerically and visually. However, some future works are planned to further increase EDOF microscope capacity. These works can be summarized as follows:

1. As mentioned in previous sections, the memory of our GPU is quite lower than other studies developing deep learning and CNN-based techniques in image processing, computer vision, and medical imaging analysis. We think that more satisfactory performance can be achieved with high-capacity hardware.
2. An auto-encoder model is created in the training stage to acquire high-dimensional attributes of multi-focus

images. This auto-encoder model consists of only convolutional and cSE blocks. We hope that utilizing additional sophisticated models, such as vision transformer [44] and Swin Transformer [45], which are more effective than cSE, will improve the deep features' strength and generalizability.

3. To assess the efficacy of the proposed EDOF microscope approach, a data set of synthetic and real microscope image collections is produced. We anticipate that extending the data set will yield more objective results.

Author Contributions All authors contributed to the study conception and design. Specimen preparation, data collection, and analysis were performed by Hulya Dogan, Ilyas Ay, and Sena F. Sezen. Synthetic data set preparation was performed by Hulya Dogan and Ramazan Ozgur Dogan. Conceptualization, methodology, software, and validation of the proposed EDOF approach were performed by Hulya Dogan and Ramazan Ozgur Dogan. The first draft of the manuscript was written by Hulya Dogan, and writing—review and editing were performed by all authors. All authors read and approved the final manuscript.

Funding We thank Karadeniz Technical University Drug and Pharmaceutical Technology Application & Research Center for their support. Part of this study was supported by a grant from the Scientific Research Project Coordination Unit of Karadeniz Technical University, Turkiye (Project no. TSA-2019-8561) and the Republic of Turkiye Ministry of Agriculture and Forestry General Directorate of Agricultural Research and Policies (Project no. TAGEM-19/AR-GE/07).

Data Availability The multi-focus image data set generated to provide comprehensive and specimen-free performance analysis of EDOF approaches during the current study are not publicly available.

Code Availability The code implementation for the EDOF approach can be obtained by contacting the first author of this paper.

Declarations

Ethics Approval The experimental protocols used in this paper were ethically approved by the Institutional Animal Ethical Committee (2019/45). All animal studies were performed according to the Guide for the Care and Use of Laboratory Animals.

Consent to Participate This study did not use human subjects.

Consent for Publication This study did not use individual person's data.

Competing Interests The authors declare no competing interests.

References

1. Ambikumar, A.S., Bailey, D.G., Gupta, G.S.: Extending the depth of field in microscopy: A review. In: 2016 International Conference on Image and Vision Computing New Zealand (IVCNZ), pp. 1–6 (2016). IEEE
2. Dowski, E.R., Cathey, W.T.: Extended depth of field through wave-front coding. Applied optics **34**(11), 1859–1866 (1995)
3. Akpinar, U., Sahin, E., Meem, M., Menon, R., Gotchev, A.: Learning wavefront coding for extended depth of field imaging. IEEE transactions on image processing **30**, 3307–3320 (2021)
4. Mo, X., Zhang, T., Wang, B., Huang, X., Kuang, C., Liu, X.: Alleviating image artifacts in wavefront coding extended depth of field imaging system. Optics Communications **436**, 232–238 (2019)
5. Cohen, N., Yang, S., Andalman, A., Broxton, M., Grosenick, L., Deisseroth, K., Horowitz, M., Levoy, M.: Enhancing the performance of the light field microscope using wavefront coding. Optics express **22**(20), 24817–24839 (2014)
6. Hermessi, H., Mourali, O., Zagrouba, E.: Multimodal medical image fusion review: Theoretical background and recent advances. Signal Processing **183**, 108036 (2021)
7. Huang, B., Yang, F., Yin, M., Mo, X., Zhong, C.: A review of multimodal medical image fusion techniques. Computational and mathematical methods in medicine **2020** (2020)
8. Pertuz, S., Puig, D., Garcia, M.A.: Analysis of focus measure operators for shape-from-focus. Pattern Recognition **46**(5), 1415–1432 (2013)
9. Pan, C., Chen, J., Zhang, R., Zhuang, S.: Extension ratio of depth of field by wavefront coding method. Optics express **16**(17), 13364–13371 (2008)
10. Zhao, T., Mauger, T., Li, G.: Optimization of wavefront-coded infinity-corrected microscope systems with extended depth of field. Biomedical optics express **4**(8), 1464–1471 (2013)
11. Gierlak, M., Albrecht, S., Kauer, J., Leverenz, E., Beckers, I.E.: Wavefront coding using a spatial light modulator for extended depth of field microscopy. In: European Conference on Biomedical Optics, p. 879803 (2013). Optica Publishing Group
12. Cao, Z., Zhai, C., Li, J., Xian, F., Pei, S.: Combination of color coding and wavefront coding for extended depth of field. Optics Communications **392**, 252–257 (2017)
13. Elmalem, S., Giryes, R., Marom, E.: Learned phase coded aperture for the benefit of depth of field extension. Optics express **26**(12), 15316–15331 (2018)
14. Du, H., Dong, L., Liu, M., Zhao, Y., Wu, Y., Li, X., Jia, W., Liu, X., Hui, M., Kong, L.: Increasing aperture and depth of field simultaneously with wavefront coding technology. Applied Optics **58**(17), 4746–4752 (2019)
15. Wei, X., Han, J., Xie, S., Yang, B., Wan, X., Zhang, W.: Experimental analysis of a wavefront coding system with a phase plate in different surfaces. Applied Optics **58**(33), 9195–9200 (2019)
16. Li, Y., Wang, J., Zhang, X., Hu, K., Ye, L., Gao, M., Cao, Y., Xu, M.: Extended depth-of-field infrared imaging with deeply learned wavefront coding. Optics Express **30**(22), 40018–40031 (2022)
17. Valdecasas, A.G., Marshall, D., Becerra, J.M., Terrero, J.: On the extended depth of focus algorithms for bright field microscopy. Micron **32**(6), 559–569 (2001)
18. Aguet, F., Van De Ville, D., Unser, M.: Model-based 2.5-d deconvolution for extended depth of field in brightfield microscopy. IEEE Transactions on Image Processing **17**(7), 1144–1153 (2008)
19. Forster, B., Van De Ville, D., Berent, J., Sage, D., Unser, M.: Complex wavelets for extended depth-of-field: A new method for the fusion of multichannel microscopy images. Microscopy research and technique **65**(1-2), 33–42 (2004)
20. Tessens, L., Ledda, A., Pizurica, A., Philips, W.: Extending the depth of field in microscopy through curvelet-based frequency-adaptive image fusion. In: 2007 IEEE International Conference on Acoustics, Speech and Signal Processing-ICASSP'07, vol. 1, p. 861 (2007). IEEE
21. Dogan, H., Baykal, E., Ekinci, M., Ercin, M.E., Ersoz, S.: A novel extended depth of field process based on nonsubsampled shearlet transform by estimating optimal range in microscopic systems. Optics Communications **429**, 88–99 (2018)

22. Costa, M.G.F., Pinto, K., Fujimoto, L.B., Ogusku, M.M., Costa Filho, C.F.: Multi-focus image fusion for bacilli images in conventional sputum smear microscopy for tuberculosis. Biomedical Signal Processing and Control **49**, 289–297 (2019)
23. Piccinini, F., Tesei, A., Zoli, W., Bevilacqua, A.: Extended depth of focus in optical microscopy: Assessment of existing methods and a new proposal. Microscopy research and technique **75**(11), 1582–1592 (2012)
24. Chen, J., Li, X., Luo, L., Mei, X., Ma, J.: Infrared and visible image fusion based on target-enhanced multiscale transform decomposition. Information Sciences **508**, 64–78 (2020)
25. Li, L., Si, Y., Wang, L., Jia, Z., Ma, H.: A novel approach for multi-focus image fusion based on sf-papcnn and isml in nsst domain. Multimedia Tools and Applications **79**, 24303–24328 (2020)
26. Ramlal, S.D., Sachdeva, J., Ahuja, C.K., Khandelwal, N.: An improved multimodal medical image fusion scheme based on hybrid combination of nonsubsampled contourlet transform and stationary wavelet transform. International Journal of Imaging Systems and Technology **29**(2), 146–160 (2019)
27. Tan, W., Tiwari, P., Pandey, H.M., Moreira, C., Jaiswal, A.K.: Multimodal medical image fusion algorithm in the era of big data. Neural Computing and Applications, 1–21 (2020)
28. Hermessi, H., Mourali, O., Zagrouba, E.: Multimodal medical image fusion review: Theoretical background and recent advances. Signal Processing **183**, 108036 (2021)
29. Liu, Y., Wang, L., Cheng, J., Li, C., Chen, X.: Multi-focus image fusion: A survey of the state of the art. Information Fusion **64**, 71–91 (2020)
30. Wang, K., Zheng, M., Wei, H., Qi, G., Li, Y.: Multi-modality medical image fusion using convolutional neural network and contrast pyramid. Sensors **20**(8), 2169 (2020)
31. Jose, J., Gautam, N., Tiwari, M., Tiwari, T., Suresh, A., Sundararaj, V., Rejeesh, M.: An image quality enhancement scheme employing adolescent identity search algorithm in the nsst domain for multimodal medical image fusion. Biomedical Signal Processing and Control **66**, 102480 (2021)
32. Liu, S., Wang, M., Yin, L., Sun, X., Zhang, Y.-D., Zhao, J.: Two-scale multimodal medical image fusion based on structure preservation. Frontiers in Computational Neuroscience **15**, 133 (2022)
33. Ye, F., Li, X., Zhang, X.: Fusioncnn: a remote sensing image fusion algorithm based on deep convolutional neural networks. Multimedia Tools and Applications **78**, 14683–14703 (2019)
34. Huang, M., Liu, S., Li, Z., Feng, S., Wu, D., Wu, Y., Shu, F.: Remote sensing image fusion algorithm based on two-stream fusion network and residual channel attention mechanism. Wireless Communications and Mobile Computing **2022**, 1–14 (2022)
35. Wang, W., Han, C., Zhou, T., Liu, D.: Visual recognition with deep nearest centroids. arXiv preprint arXiv:2209.07383 (2022)
36. Salahuddin, Z., Woodruff, H.C., Chatterjee, A., Lambin, P.: Transparency of deep neural networks for medical image analysis: A review of interpretability methods. Computers in biology and medicine **140**, 105111 (2022)
37. Fan, F.-L., Xiong, J., Li, M., Wang, G.: On interpretability of artificial neural networks: A survey. IEEE Transactions on Radiation and Plasma Medical Sciences **5**(6), 741–760 (2021)
38. Dong, S., Gao, Z., Pirbhulal, S., Bian, G.-B., Zhang, H., Wu, W., Li, S.: Iot-based 3d convolution for video salient object detection. Neural computing and applications **32**, 735–746 (2020)
39. Shang, R., Chen, C., Wang, G., Jiao, L., Okoth, M.A., Stolkin, R.: A thumbnail-based hierarchical fuzzy clustering algorithm for sar image segmentation. Signal Processing **171**, 107518 (2020)
40. Venkatanath, N., Praneeth, D., Bh, M.C., Channappayya, S.S., Medasani, S.S.: Blind image quality evaluation using perception based features. In: 2015 Twenty First National Conference on Communications (NCC), pp. 1–6 (2015). IEEE
41. Mittal, A., Moorthy, A.K., Bovik, A.C.: No-reference image quality assessment in the spatial domain. IEEE Transactions on image processing **21**(12), 4695–4708 (2012)
42. Mittal, A., Soundararajan, R., Bovik, A.C.: Making a completely blind image quality analyzer. IEEE Signal processing letters **20**(3), 209–212 (2012)
43. Lin, T.-Y., Maire, M., Belongie, S., Hays, J., Perona, P., Ramanan, D., Dollár, P., Zitnick, C.L.: Microsoft coco: Common objects in context. In: European Conference on Computer Vision, pp. 740–755 (2014). Springer
44. Dosovitskiy, A., Beyer, L., Kolesnikov, A., Weissenborn, D., Zhai, X., Unterthiner, T., Dehghani, M., Minderer, M., Heigold, G., Gelly, S., et al.: An image is worth 16x16 words: Transformers for image recognition at scale. arXiv preprint arXiv:2010.11929 (2020)
45. Liu, Z., Lin, Y., Cao, Y., Hu, H., Wei, Y., Zhang, Z., Lin, S., Guo, B.: Swin transformer: Hierarchical vision transformer using shifted windows. In: Proceedings of the IEEE/CVF International Conference on Computer Vision, pp. 10012–10022 (2021)

Authors and Affiliations

Hulya Dogan[1,3] · Ramazan Ozgur Dogan[2] · Ilyas Ay[3] · Sena F. Sezen[3,4]

✉ Hulya Dogan
hulya@ktu.edu.tr

Ramazan Ozgur Dogan
ramazan.dogan@gumushane.edu.tr

Ilyas Ay
ilyas.ay@ktu.edu.tr

Sena F. Sezen
senasezen@ktu.edu.tr

[1] Department of Software Engineering, Faculty of Engineering, Karadeniz Technical University, Trabzon 61080, Türkiye

[2] Department of Software Engineering, Faculty of Engineering and Natural Sciences, Gumushane University, Gumushane 29100, Türkiye

[3] Drug and Pharmaceutical Technology Application & Research Center, Karadeniz Technical University, Trabzon 61080, Türkiye

[4] Department of Pharmacology, Faculty of Pharmacy, Karadeniz Technical University, Trabzon 61080, Türkiye